

Rotation of the Conduction Band Valleys in AlAs due to X_X - X_Y Mixing

Hyunsik Im,¹ P. C. Klipstein,^{1,*} R. Grey,² and G. Hill²

¹*Clarendon Laboratory, Department of Physics, University of Oxford, Parks Road, Oxford OX1 3PU, United Kingdom*

²*EPSRC III-V Semiconductor Facility, Department of Electrical and Electronic Engineering, University of Sheffield, Mappin Street, Sheffield S1 3JD, United Kingdom*

(Received 10 December 1998)

We report resonant magnetotunneling measurements of the energy dispersion near the third X symmetry subband edge in 60 and 70 Å thick AlAs quantum wells with GaAs barriers, grown along $z = [001]$. An elliptical constant energy surface is observed, oriented parallel to either $[110]$ or $[\bar{1}10]$. This rotation of 45° with respect to the bulk AlAs Fermi surface is explained by interface induced X_X - X_Y mixing. Our results provide new insight into both Γ - X_Z and X_X - X_Y mixing, showing conclusively that states with both X_1 and X_3 symmetry contribute. This contrasts with several recent theoretical studies in which the X_1 contribution is zero.

PACS numbers: 73.20.Dx, 71.18.+y, 73.40.Gk

In semiconductor heterostructures (e.g., GaAs/AlAs) grown along z ($[001]$), mixing between states of different symmetry, such as Γ and X_Z , has been the subject of many experimental and theoretical studies (e.g., [1] and references therein [2–5]). While such mixing is known to be interface related, until recently virtually no study provided insight into its microscopic origin. Theoretical predictions relied either on a detailed band structure calculation for the complete heterostructure [2,3,5] or on a phenomenological approach in which the mixing was represented by experimentally fitted constants in an effective mass model [4,6]. Some full calculations showed that the mixing was sensitive to N and M , the number of GaAs and AlAs monolayers, respectively [3]. This was explained on purely symmetry grounds by Aleiner and Ivchenko [7], and incorporated successfully into an effective mass model [4]. However, contrary to Ref. [2], it was assumed in Refs. [4] and [7] that only mixing with the upper X_3 symmetry band was important, based on the theoretical results of Ando and Akera [5]. The X_3 band lies $\Delta \sim 0.35$ eV above the lower X_1 symmetry band that forms the conduction band edge in AlAs, and $\mathbf{k} \cdot \mathbf{p}$ mixing between X_1 and X_3 was invoked to explain the observed mixing between Γ and X_Z states in the band edge region [4].

Very recently, two theoretical studies have provided the most direct insight into the origin of the mixing, relating it to the microscopic symmetry of the crystal potential in the vicinity of the interface [8,9]. From Ref. [8] it becomes clear that the X_1 contribution to Γ - X_Z mixing is not necessarily zero, while both studies show that the *same* microscopic potential that mixes Γ and X_Z can also mix X_X and X_Y . Mixing between X_X and X_Y was demonstrated theoretically as long ago as 1989 [3] but to the best of our knowledge it has never been observed experimentally. In this Letter, we present the first such observation based on the fact that in an AlAs quantum well, X_X - X_Y mixing can lead to a reorientation of the two dimensional constant energy surface along one

of the $\langle 110 \rangle$ directions. We derive a formula for the dispersion which shows that the reorientation is a direct consequence of the constructive interference between the X_1 and X_3 contributions for one of the $\langle 110 \rangle$ directions and destructive for the other. Thus our result also proves that the X_1 contribution, both to X_X - X_Y and Γ - X_Z mixing, is important. From the shape of the constant energy surface we are able to estimate the relative sizes of the X_1 and X_3 contributions.

We have performed measurements as a function of the angle of an in-plane magnetic field, of $2D \rightarrow 2D$ tunneling between confined X states in GaAs/AlAs structures with 60 or 70 Å wide AlAs wells and a 30 or 40 Å wide GaAs barrier. Experimental details are described in Ref. [10]. The magnetic field introduces a change in wave vector during tunneling, $\Delta k_y = -eB_x \Delta z / \hbar$, which allows the collector dispersion to be measured from the shift in bias produced by the field [11,12]. Here, Δz is the distance between the emitter and collector wave functions. For both of the present samples at 15 T, $\Delta k_y \sim 0.02$ in units of $2\pi/a_0$, where a_0 is the cubic lattice constant. High pressure, a large bias, or a compositionally graded $\text{Al}_x\text{Ga}_{1-x}\text{As}$ emitter, can be used to populate the $X_{X,Y}$ ground state in the emitter AlAs well with electrons from a doped GaAs contact separated by a spacer layer [10].

Figure 1 shows dI/dV vs V for a sample with 70 Å AlAs wells and a 30 Å GaAs barrier, whose design is otherwise identical to the samples in Ref. [10], except that the GaAs region before each spacer has been linearly graded with aluminum over a distance of 1000 Å to $\text{Ga}_{0.9}\text{Al}_{0.1}\text{As}$, which is also the spacer composition. The $X_{X,Y}(1) \rightarrow X_{X,Y}(m)$ processes responsible for the peaks in Fig. 1 may be identified by comparison of their bias values with those of a similar but ungraded sample analyzed in detail in Ref. [10]. Transport of electrons from emitter to collector takes place by quantum beats between double well states, as discussed in Ref. [1].

Figure 1 shows that the $X_{X,Y}(1) \rightarrow X_{X,Y}(3)$ peak shifts to higher bias with increasing magnetic field, applied

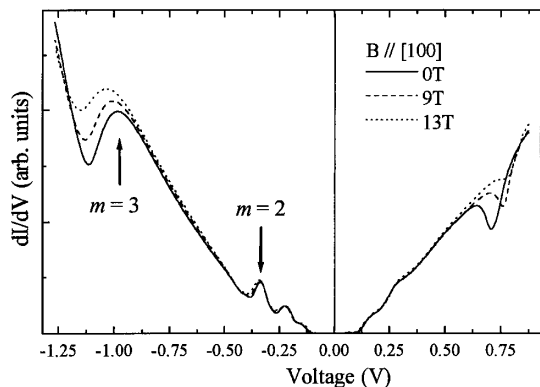


FIG. 1. Conductance vs bias at 4.2 K for the 70-30-70 sample. Magnetic fields of 0 T (solid line), 9 T (dashed line), and 13 T (dotted line) are applied in the [100] direction. $X_{X,Y}(1) \rightarrow X_{X,Y}(m)$ processes are indicated for reverse bias, where m is the confinement quantum number in the collector well.

parallel to [100]. In Fig. 2, the bias shift is plotted for all in-plane field angles. A dumbbell is observed whose orientation, along a $\langle 110 \rangle$ direction, is identical for both bias directions. In reverse bias the ratio of shifts for the two $\langle 110 \rangle$ directions is significantly larger (2.8 at 15 T, 3.7 at 12 T) than in forward bias (1.6 at 10.5 T). This ratio varied between different mesas from the same wafer, particularly in reverse bias, where for three mesas the largest value at 15 T was 2.8, and the smallest 1.9. Identical measurements were made on a 60-40-60 sample with an ungraded emitter and collector [10]. In this case, the major dumbbell axis was also oriented along a $\langle 110 \rangle$ direction but it rotated by 90° with bias direction. The ratio of shifts at 15 T for the two $\langle 110 \rangle$ directions was 1.4 and 1.2, respectively, in forward and reverse bias.

The dumbbells observed for the two samples and bias directions correspond to elliptical constant energy surfaces in the collector well, with axes oriented along the $\langle 110 \rangle$ directions, as shown schematically in Fig. 3. This follows from the direct relationship between bias shift and dispersion in the collector well, which holds for two reasons. First, the splittings between the energies of the symmetric and the antisymmetric *double well* wave functions for the $m = 3$ resonance in zero magnetic field (~ 0.75 meV for 70-30-70 and ~ 0.28 meV for 60-40-60) are smaller than the typical collector kinetic energies at $k_{\parallel} \sim 0.02$ (plotted in Fig. 4). Second, any diamagnetic shifts of the single well confinement energies are very small [11].

In the bulk, $\mathbf{k} \cdot \mathbf{p}$ mixing between the $X_{1\sigma}$ and $X_{3\sigma}$ states produces the familiar camel's back dispersion along k_{σ} , where $\sigma = x, y, \text{ or } z$. The respective amplitudes of $X_{1\sigma}$ and $X_{3\sigma}$ states, $b(k_{\sigma})$ and $a(k_{\sigma})$, can be found in Ref. [4], expressed in terms of the X_1 - X_3 energy splitting, Δ , and the $\mathbf{k} \cdot \mathbf{p}$ interaction parameter, R . In a heterostructure, the interfaces may cause mixing between confined X_X and X_Y states, with wave functions,

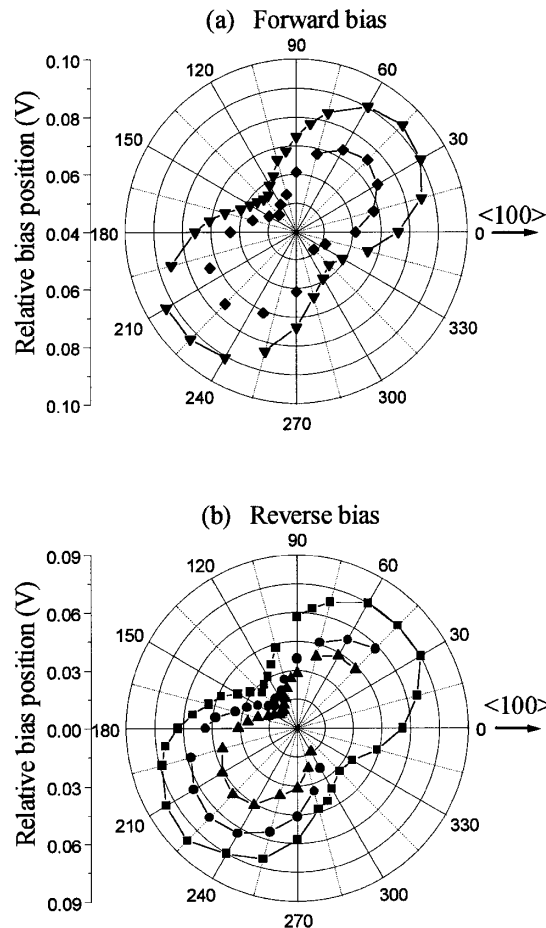


FIG. 2. Bias shift of the $X_{X,Y}(1) \rightarrow X_{X,Y}(3)$ peak of the 70-30-70 sample with magnetic field angle for (a) forward and (b) reverse biases, 0° and 90° correspond to the $\langle 100 \rangle$ directions (diamond: 9 T; down triangle: 10.5 T; up triangle: 12 T; circle: 13.5 T; square: 15 T).

$$\Psi_{X_{\sigma}} = \{ \Xi_{\sigma}(z) b(k_{\sigma}) u_{X_{1\sigma}} + \hat{\Xi}_{\sigma}(z) a(k_{\sigma}) u_{X_{3\sigma}} + \dots \} e^{ik_{\parallel} r}, \quad (1)$$

where $\sigma = X$ or Y [4,8]. Here $u_{X_{1\sigma}}$ and $u_{X_{3\sigma}}$ are the $k_{\parallel} = 0$ lattice periodic functions associated with the X_1, X_3 manifold of the *average* bulk crystal, and the dots in Eq. (1) represent the small contribution of the remote bands outside this manifold [8]. $\Xi_{\sigma}(z), \hat{\Xi}_{\sigma}(z)$ are the dominant envelope functions for the X_1, X_3 potential wells, respectively. In the following we assume $\Xi_{\sigma}(z) \approx \hat{\Xi}_{\sigma}(z)$ since the X_1 and X_3 well depths and confinement masses are thought to be fairly similar [4]. For interfaces at z_i the mixing matrix element is [4,8]

$$V(k_x, k_y) = b^*(k_x) b(k_y) \bar{V}_1^{X-Y} + a^*(k_x) a(k_y) \bar{V}_3^{X-Y}, \quad (2)$$

where $\bar{V}_s^{X-Y} = \sum_{z_i} \Xi_X^*(z_i) \Xi_Y(z_i) V_s^{X-Y}(z_i)$, in which $V_1^{X-Y}(z_i) = \beta_1 \cdot \eta(z_i)$ and $V_3^{X-Y}(z_i) = \beta_3 \cdot \eta(z_i) \cdot P(z_i)$, with constants $\beta_1 < \beta_3$. The phase factor, $\eta(z_i) =$

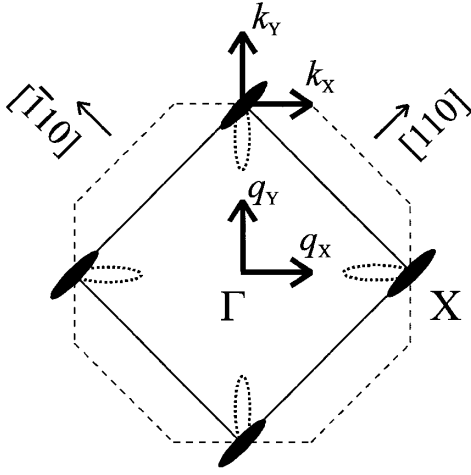


FIG. 3. Schematic 2D Brillouin zone and constant energy surface superimposed on the $(q_x, q_y, 0)$ cross section of the bulk AlAs Brillouin zone (dashed line) and Fermi surface (dotted line). The bulk Γ and X points are indicated.

$\exp(i2\pi z_i/a_0)$ alternates between ± 1 with each displacement of a monolayer along z . Attention is drawn to the factor $P(z_i) = 1$ for a normal interface (AlAs on GaAs), -1 for an inverted interface (GaAs on AlAs) (which is missing from Ref. [4]) [13].

The mixed state energies are found by diagonalizing the 2×2 Hamiltonian, \underline{H} , in which

$$H_{11} = \frac{\hbar^2}{2} \left[\frac{k_x^2}{m_Z'} + \frac{k_y^2}{m_{X,Y}} \right] - E_{\mathbf{k} \cdot \mathbf{p}}(k_x),$$

$$H_{22} = \frac{\hbar^2}{2} \left[\frac{k_x^2}{m_{X,Y}} + \frac{k_y^2}{m_Z'} \right] - E_{\mathbf{k} \cdot \mathbf{p}}(k_y),$$

$$H_{12} = H_{21}^* = V, \quad \text{and} \quad E_{\mathbf{k} \cdot \mathbf{p}}(k_\sigma) = \sqrt{(\Delta/2)^2 + R^2 k_\sigma^2}.$$

Here H_{11} and H_{22} are the bulk dispersions with $m_{X,Y}/m_e = 0.24$ [10,14]. Figure 4 shows the $[110]$, $[010]$, and $[\bar{1}10]$ dispersions calculated with $R = 1 \text{ eV \AA}$ and $m_Z'/m_e \approx 1.56$ [4]. Note that along $[010]$ the dispersion is independent of \bar{V}_3^{X-Y} because $a^*(k_x)a(k_y) = 0$. A value

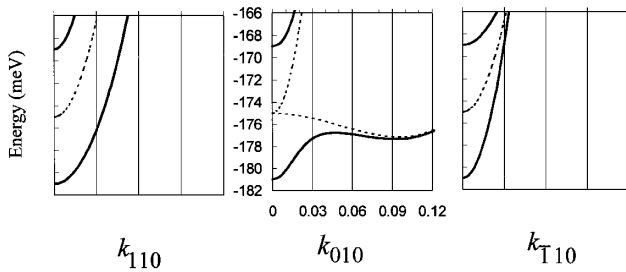


FIG. 4. Dispersions in the $[110]$, $[010]$, and $[\bar{1}10]$ in-plane directions for $\bar{V}_1^{X-Y} = 6 \text{ meV}$, $\bar{V}_3^{X-Y} = 850 \text{ meV}$ (solid line), and $\bar{V}_1^{X-Y} = \bar{V}_3^{X-Y} = 0 \text{ meV}$ (dashed line). Zero energy is midway between the bulk X_1 and X_3 edges.

of $\bar{V}_3^{X-Y} = 850 \text{ meV}$ was chosen in Fig. 4, to give a ratio of $\langle 110 \rangle$ effective masses for $k_{\parallel} \leq 0.02$ equal to 2.8, the ratio of the major to minor axes at 15 T in Fig. 2(b) [15]. This mass ratio is quite insensitive to \bar{V}_1^{X-Y} . In Fig. 4, we have used $\bar{V}_1^{X-Y} = 6 \text{ meV}$ [16], but an optimum value of $\bar{V}_1^{X-Y} \sim 30 \text{ meV}$ is found to reproduce the shape of the dumbbell in Fig. 2(b) quite well [17].

For consistency with Ref. [4], we have used the values of R and m_Z' given there but we suspect that they are not correct because they cannot explain the confinement energies observed for the $X_Z(1)$ state in quantum wells with widths between 20 and 40 \AA . The confinement wave vectors corresponding to these widths are approximately 0.14 and 0.07, respectively (infinite well depth approximation) while the confinement energy of the 20 \AA well is $\sim 65 \text{ meV}$ greater than that of the 40 \AA [18]. This is not consistent with the form of the *bulk* camel's back, shown as a dashed line in Fig. 4, which has a minimum at $k_{010} \sim 0.10$, and so we suggest that a reevaluation is needed. We find that $R = 2.5 \text{ eV \AA}$ and $m_Z'/m_e = 0.3$ gives a camel's back with a minimum at $k_{010} \sim 0.06$ and a depth of 10 meV that is more consistent with Ref. [18]. Using these parameters, a good fit to the angular dependence of the kinetic energy in Fig. 2(b) is obtained for $\bar{V}_1^{X-Y} = 30 \text{ meV}$ and $\bar{V}_3^{X-Y} = 120 \text{ meV}$. As before, \bar{V}_3^{X-Y} determines the ratio of kinetic energies in the two $\langle 110 \rangle$ directions, while \bar{V}_1^{X-Y} determines the kinetic energy variation at all other angles. Notably, \bar{V}_1^{X-Y} appears much less sensitive than \bar{V}_3^{X-Y} to the choice of the bulk $\mathbf{k} \cdot \mathbf{p}$ parameters.

We have calculated the amplitudes of the envelope functions for the $m = 3$ resonance at the four GaAs/AlAs interfaces ($i = 1, 2, 3$, and 4) as in Ref. [10] assuming that the charge stored in the emitter well is twice that in the collector. This is a reasonable assumption for the present qualitative analysis. For the 70-30-70 and the 60-40-60 samples, the squared amplitudes at the two collector interfaces are in the ratio $S:1$ with $S = 0.63$ and 0.76, respectively. Writing $\bar{V}_1^{X-Y} = \beta_1 A$ and $\bar{V}_3^{X-Y} = \beta_3 B$, we have $B/A = [S\eta(z_3)P(z_3) + 1 \times \eta(z_4)P(z_4)]/[S\eta(z_3) + 1 \times \eta(z_4)]$ in one bias direction and $B/A = [1 \times \eta(z_1)P(z_1) + S\eta(z_2)P(z_2)]/[1 \times \eta(z_1) + S\eta(z_2)]$ in the other. With M odd (even) this gives B/A (A/B) ~ -7.3 and 7.3, respectively, for the two bias directions in a sample with perfect interfaces and dimensions close to 60-40-60. The change of sign is consistent with the rotation of the dumbbell by 90° observed in the 60-40-60 sample when the bias is reversed. For imperfect interfaces, however, we consider the case when the normal interfaces ($i = 2, 4$) contribute much more than the inverted ($i = 1, 3$), or vice versa, for example, due to different degrees of roughness [19]. Then $|B/A| \sim 1$, and there is no rotation. This could explain the absence of a rotation for the 70-30-70 sample in Fig. 2. For the two bias directions, the ratio of $|B|$ values is then $1:S$, consistent with the different ratios of major to minor axes in Fig. 2.

Assuming $|B/A| \sim 1$ for the 70-30-70 sample, $\bar{V}_1^{X-Y} = 30$ meV, $\bar{V}_3^{X-Y} = 120$ meV, correspond to $\beta_1 \sim 1.2$ eV Å, $\beta_3 \sim 4.8$ eV Å. In comparison, Lu and Sham's model for $X_{X,Y}(1)$ in ~ 30 Å AlAs wells gives $\bar{V}_1^{X-Y} \sim 8$ meV, or $\beta_1 \sim 0.4$ eV Å [3]. They did not include the X_3 band in their calculation. This magnitude for β_1 is consistent with ours considering the simplicity of the model for the interface potential in Ref. [3] and the uncertainty in the ratio of $|B/A|$ and the bulk $\mathbf{k} \cdot \mathbf{p}$ parameters in our case. However, a finite β_1 is not consistent with the zero prediction in Ref. [9]. This apparent discrepancy can be explained by considering the detailed form of the interface potential [8]. For β_3 , Ref. [9] predicts a value of ~ 0.5 eV Å. This value is much smaller than our experimental estimate, even allowing for the uncertainties discussed above. Present envelope function models may thus require further refinement.

In conclusion, we have observed the first clear evidence for mixing between AlAs X_X and X_Y states predicted in Ref. [3]. We have shown that the mixing leads to a rotation of the constant energy surface from the two in-plane $\langle 100 \rangle$ directions to one of the $\langle 110 \rangle$ directions. The rotation is a consequence of interference between the X_1 and X_3 related mixing potentials, so that both must be finite. We find that their values are significantly larger than predicted by present envelope function theories. Since the X_X - X_Y mixing potentials are closely analogous to corresponding potentials for Γ - X_Z mixing [8], our results also imply that the X_1 related potential for Γ - X_Z mixing, which is usually taken to be zero [4,5,9], may in fact be finite.

This work was funded by the E.P.S.R.C. of the U.K. and H.I. acknowledges support from the LG Semicon. Co. Ltd. P.C.K. acknowledges a useful discussion with Professor E.L. Ivchenko. We thank L.E. Bremme for a critical reading of the manuscript.

*Presently visiting the Weizmann Institute, Rehovot, Israel.

[1] P.C. Klipstein, in *Tunneling under Pressure*, edited by T. Suski and W. Paul, Semiconductors and Semimetals Vol. 55 (Academic Press, New York, 1998), Chap. 2, pp. 45–116.

- [2] L.-W. Wang, A. Franceschetti, and A. Zunger, Phys. Rev. Lett. **78**, 2819 (1997); L.-W. Wang and A. Zunger, Phys. Rev. B **56**, 12 395 (1997).
- [3] Y.-T. Lu and L.J. Sham, Phys. Rev. B **40**, 5567 (1989).
- [4] Y. Fu, M. Willander, E.L. Ivchenko, and A.A. Kiselev, Phys. Rev. B **47**, 13 498 (1993).
- [5] T. Ando and H. Akera, Phys. Rev. B **40**, 11 619 (1989).
- [6] J.-B. Xia, Phys. Rev. B **41**, 3117 (1990).
- [7] I.A. Aleiner and E.L. Ivchenko, Fiz. Tekh. Poluprovodn. **27**, 594 (1993) [Sov. Phys. Semicond. **27**, 330 (1993)].
- [8] P.C. Klipstein, in *Proceedings of the 24th International Conference on The Physics of Semiconductors*, edited by M. Heiblum and E. Cohen (World Scientific, Singapore, 1998); CDROM file: 1265.pdf (1999).
- [9] B.A. Foreman, Phys. Rev. Lett. **81**, 425 (1998).
- [10] J.M. Smith, P.C. Klipstein, R. Grey, and G. Hill, Phys. Rev. B **57**, 1740 (1998).
- [11] R.K. Hayden *et al.*, Phys. Rev. Lett. **66**, 1749 (1991).
- [12] J.M. Smith, P.C. Klipstein, R. Grey, and G. Hill, Phys. Rev. B **58**, 4708 (1998).
- [13] In the notation of Ref. [4], the S_4 operation changes, the sign of d/dz , u_x to u_y , u_y to u_x , v_x to v_y , and v_y to $-v_x$. The last pair of changes makes the second of boundary conditions (3.2a) in Ref. [4] invariant under S_4 , so that the second of boundary conditions (3.2b) has the wrong sign in front of $t_{xy}^{(v)}$. A factor $\zeta_l^{(v)}$, which has opposite signs for an AB and a BA interface, is thus needed in Eq. (3.4) in front of $U^{(v)}$, analogous to ζ_l for the case of Γ - X_Z mixing in Eq. (2.8). This factor is the same as $P(z_i)$ here and in Ref. [8] [note also that \hat{I} in Eq. (3.4) is the Pauli σ_X matrix, not the unit matrix as stated].
- [14] H. Im, P.C. Klipstein, R. Grey, and G. Hill, in *Proceedings of the 24th International Conference on The Physics of Semiconductors* (Ref. [8]); CDROM file: 1075.pdf (1999).
- [15] The weak dependence of this ratio on magnetic field may be due to nonparabolicity and to the more complex dependence of bias shift on field when Δk_y is comparable to the Fermi wave vector of electrons in the emitter.
- [16] This value was used in Fig. 5 of Ref. [4].
- [17] H. Im, L.E. Bremme, Y.C. Chung, P.C. Klipstein, R. Grey, and G. Hill, Physica (Amsterdam) E (to be published).
- [18] H. Im, P.C. Klipstein, J.M. Smith, R. Grey, and G. Hill, Phys. Status Solidi (b) **211**, 489 (1998).
- [19] Note that the value of $\eta(z_i)$ averaged over the effective area of a given interface is very sensitive to the presence of steps, because a monolayer step reverses the sign of η .